# A Native Mass Spectrometry Approach to Qualitatively Elucidate Interfacial Epitopes of Transient Protein-Protein Interactions

Clinton G. L. Veale,*[a] Abir Chakraborty,[b] Richwell Mhlanga,[b] Fernando Albericio,[c] Beatriz G. de la Torre,[d] Adrienne L. Edkins,[b] and David J. Clarke*[e]

[a]Department of Chemistry, University of Cape Town, Rondebosch, Cape Town, 7701, South Africa.
[b]Biomedical Biotechnology Research Unit (BioBRU), Department of Biochemistry and Microbiology, Rhodes University, Makhanda, 6139, South Africa.
[c]School of Chemistry and Physics, University of Kwa-Zulu Natal, Westville, South Africa
[d]School of Laboratory Medicine and Medical Sciences, University of Kwa-Zulu Natal, South Africa
[e]EaStCHEM, School of Chemistry, University of Edinburgh, Joseph Black Building, David Brewster Road, Edinburgh, EH93FJ

***Correspondence:** clinton.veale@uct.ac.za, dave.clarke@ed.ac.uk

**Keywords**
Native Mass Spectrometry; Limited Proteolysis; Transient Protein-Protein Interactions; HOP-HSP90; DnaK-GrpE

**Abstract**
Native mass spectrometric analysis of TPR2A and GrpE with unpurified peptides derived from limited proteolysis of their respective PPI partners (HSP90 C-terminus and DnaK) facilitated efficient, qualitative identification of interfacial epitopes involved in transient PPI formation. Application of this approach can assist in elucidating interfaces of currently uncharacterised transient PPIs.

The central mediatory role of protein-protein interactions (PPIs) in biological processes offers significant opportunity to unravel details of disease progression and expand druggable chemical space.[1] Many biological functions including, signalling networks and regulation of biochemical pathways, rely on a subset of PPIs, where interfacial associations are comparatively weak and shorter-lived.[2] While this transient nature is a key property in their regulatory role, it also limits the ability of many structural biology techniques to observe these interfacial associations. A full understanding of the biological function and mechanism of interactions within transient PPIs, as well as the development of PPI modulators, requires detailed structural characterisation of binding interfaces, including locating and identifying interacting domains, amino acid sequences and so-called hot-spot regions.[3] Compared to strong/permeant PPIs, such as antibody-antigen interactions, which are characterised by high surface area domain – conformational epitope interactions, the primary interaction of transient PPIs commonly feature a smaller surface area interface, typically dominated by the interaction between a domain and a linear peptide motif.[4,5] These short linear motifs (SLiMs) are usually found as terminal peptides or as linear hot-segments within intrinsically disordered proteins/regions (IDP/R).[2,6] It is this property that allows peptide-protein interactions (PepPIs) to be studied as reduced complexity PPI model systems for interfacial characterisation and inhibitor design.[7]

Native mass spectrometry (MS), in which native state solution-phase structural information is transmitted into the gas phase facilitates the elucidation and quantification of weak biomolecular interactions.[8,9] Its inherent speed, sensitivity, low sample consumption and comparably simpler experimental set-up in comparison to x-ray crystallography, NMR or cryo-EM has seen its increasing up-take in structural biology.[10] Importantly, the ability of native MS to confidently discern between binding species based on specific alterations of the mass-to-charge ratio (*m/z*) is particularly useful for chemical biology and drug discovery applications and has seen it utilized to directly observe PepPIs as gas-phase PPI proxies capable of identifying PPI modulators.[11–14] Nevertheless, the *in vitro* identification of natural interfacial peptides required to construct a suitably representative Pep-PI is another substantial challenge, typically requiring some format of peptide scanning and, ultimately the synthesis of a library of overlapping

peptides.[15,16] Alternatively, biologically inspired methodologies such as phage display are uniquely powerful means of identifying binding epitopes. However, its application to PPI interfaces requires the construction of custom phage display libraries, which suitably represent the partner protein in question.[17] Therefore, the simplification of epitope mapping methodologies for PPI interfacial elucidation becomes a function of efficiently generating predictable peptides representative of a partner protein combined with the ability to detect and compare their relative interaction with the corresponding partner protein.
In a study investigating the strong antibody – antigen interaction of Amyloid β-Protein (Aβ) and an anti-Aβ antibody, Lu et. al. utilised limited digestion proteolysis to excise an 11 amino acid linear epitope from the 40 amino acid Aβ 1–40 peptide, which through native MS was confirmed to bind to the Fab region of the anti-Aβ antibody.[18]

We reasoned that a similar approach might be suitable for characterising transiently interacting proteins, where limited proteolysis would generate a suite of overlapping peptides representative of one partner protein analyte. We further surmised that a reasonably selective and predictable proteolytic enzyme would allow a crude proteolytic mixture to be directly incubated with the corresponding partner protein and analysed under native MS conditions. Here, we envisioned binding peptides could be identified directly from the crude peptide mixtures from the Δ*m/z* emanating from their predictable mass signature. Identification of both binding and non-binding peptides would provide an efficient and rapid means of estimating the likely minimal linear epitope responsible for the greatest contribution toward transient PPI interaction formation and further streamlining processes for hot-spot identification. Analysis of apo TPR2A under native MS conditions resulted in a charge state distribution consistent with a 20.6 kDa monomer (**Fig. 1A**). Limited proteolysis of the HSP90-C terminal domain (HSP90-C) was conducted using agarose-supported trypsin in a 100 mM $NH_4OAc$ solution, from which 2 µL aliquots were removed following 1h, 2h and 18h of digestion. Aliquots were directly incubated with TPR2A without further modification and analysed under native MS conditions using high-resolution nESI FT-ICR MS (**Fig. 2**).
At the 1h time point, four distinct peptide binding species (**1 – 4, Table S1**) were observed, with peptides **1**, **2** and **4** appearing as relatively minor TPR2A-binding species and peptide **3** in the largest relative abundance across all charge states (**Fig. 3, Table S2**). Binding species were unambiguously identified through Δ *m/z* analysis compared to the apo peak combined with high-resolution MS analysis of the isotope distributions of protein-peptide peaks (**Fig. 4, Table S1**). In addition, collision-induced MSMS could be used to dissociate the gas phase protein-peptide complex and directly measure the mass of the free peptide. From these data, **1** was identified as the known interfacial MEEVD peptide and **3** and **4** as larger peptides containing the MEEVD motif. Interestingly, peptide **2** was a non-MEEVD-containing analogue of **3**. Direct evidence of the binding of this region is particularly significant since a recent study utilising cryo-EM to resolve a GR–HSP90–HSP70–HOP complex omitted the majority of the sequence of peptide **2** (**Fig.5A**) from its structure,[19] possibly due to its intrinsic disorder. Native MS, following 2h of digestion, saw incremental changes in the relative abundances of all four peptide binding species, while peptides derived after 18h of digestion saw more substantial changes, where the complexes of peptides **1** and **2** with TPR2A were substantially more abundant. The TPR2A – **3** complex had reduced in abundance to be roughly equal to the TPR2A – **1** complex (**Fig. 3, Table S2**). The TPR2A – peptide **4** complex was absent after 18h, presumably a result of substantial proteolytic depletion of peptide **4**.

An LC-MS analysis of the HSP90-C peptide mixture following 18h of tryptic digestion did not contain peptide **4**. However, peptides **1 – 3** were all identifiable, alongside five additional non-binding peptides which together covered a large proportion of the HSP90-C sequence (**Fig. 5**).
We then progressed to assessing the impact that introducing interface competing ligands (**Fig. 6**) might have on the binding fingerprint of TPR2A with the 18h tryptic digest of HSP90-C.
Incubation with Ac-MEEVD (**5**) unsurprisingly resulted in competition for binding with both MEEVD-containing peptide **1** and **3** complexes, respectively, leading to a reduction in their relative abundances (**Fig. 3** and **7**). However, it was noticeable that peptides **2** and **5** could bind simultaneously, and the abundance of the TPR2A – **2** complex was virtually unaffected by the presence of peptide **5**. A tetrazole-containing Ac-MEEVD analogue (Ac-METrVD, **6**), which we had previously disclosed as a TPR2A – HSP90 C PPI inhibitor,[11,20] had a far more pronounced effect on the abundance of peptide **1** and **3** complexes, and while a minor ternary complex with TPR2A and peptides **2** and **6** was observed, peptide **6** was also able to substantially disrupt the TPR2A – **2** complex (**Fig 3** and **7**). Significantly, this indicates

that **6** can disrupt the PPI interface beyond the MEEVD interaction site, which likely underpins its previously reported PPI inhibitory activity. This further suggests that the secondary interfacial region is important for discerning between interfacial mimics and potential PPI inhibitors.

To further demonstrate our proof of concept we progressed to a second transient PPI between the mycobacterial chaperone, DnaK and its nucleotide exchange factor GrpE. DnaK and GrpE are individually essential for protein homeostasis in both *M. smegmatis* (Msm) and *M. tuberculosis* (Mtb), and as such the PPI is a promising non-canonical target for Mtb drug discovery.[21] At the time of our DnaK-GrpE experiments, the Mtb DnaK-GrpE PPI was not defined. However, a very recent report by Li and co-workers structurally resolved the DnaK – GrpE PPI, where they found that the association between Mtb DnaK and two GrpE subunits occurred at three major interfacial contact regions.[22] Having identified the three major contact regions and based on structural information, point mutations were systematically introduced to both DnaK (mutant 1: Y106A and L107A; mutant 2: E236A, Y257A; mutant 3: E359A, D362A; mutant 4: E387A, T390A, T394A and K395A **Fig. 5**) and GrpE. Generally, mutations on either GrpE or DnaK had a minor detrimental effect on PPI formation, with the exception of mutant 2. This alteration in the DnaK nucleotide binding domain (NDB) IIB subdomain, not only abolished PPI formation, but also the ability of DnaK to reactivate denatured luciferase. DnaK E236 forms a salt bridge with R169 of GrpE subunit 1 while DnaK Y257 forms dual H bonds with D110 of GrpE subunit 1 and S118 from a second subunit of GrpE.[22] Our MS analysis of GrpE under native conditions revealed a charge state distribution, consistent with a 25.3 kDa monomer (**Fig. 1B**). Importantly, the deconvoluted mass, confirmed that under these conditions, we did not observe GrpE as a dimer. Incubation of an aliquot of DnaK derived peptides following an 18-hour tryptic digest resulted in the binding of two DnaK peptides (**7** and **8**, **Fig. 8** and **9, Table S1**). Both peptides shared substantial sequence overlap and originated from the DnaK NBD-IIB subdomain and contained the E236 hot-spot residue, which was removed in mutant 2. LC-MS analysis of the DnaK digest showed that overlapping peptides covering the majority of the DnaK sequence were obtained, including all PPI contact regions (**Fig. 5**).

Significantly, no GrpE binding was observed for any of these peptides, supporting the notion that subdomain NBD-IIB represents the key PPI interfacial region. While no single peptide containing both the E236 and Y257 residues was identified, two peptides encompassing Y257 were identified, but whose GrpE binding was not observed. However, given that Y257 interacts at the GrpE dimer interface, the lack of dimerization likely hampered peptide binding.

In conclusion, we have demonstrated a resource-efficient approach, that, with simple sample manipulation, could qualitatively identify peptides associated with the TPR2A – HSP90-C PPI including a novel secondary interfacial region of the TPR2A – HSP90-C PPI whose interaction with TPR2A was previously unresolved through cryo-EM. Furthermore, we observed Pep-PIs representing the core DnaK-GrpE PPI region, with the subsequent cryo-EM structure providing validation for our unbiased observations. In addition to reinforcing the capacity of native MS for identifying weakly interacting interfaces, the ability to observe the secondary interfacial interaction is significant since it provides new insight into the TPR2A – HSP90 C-terminal PPI formation and disruption mechanisms. Similarly, identification of the GrpE interfacial peptides provides a starting point for the development of probes capable of modulating this biologically important PPI. Challenges associated with the generation of representative peptide libraries, alongside the technical limitations of many common biophysical techniques, significantly hinders our ability to understand and exploit these fundamental biological interactions. *In silico* methodologies have emerged perforce as the benchmark for predicting interfacial SLiMs of transient PPIs.[23] Whilst undoubtedly powerful, the development of *in vitro* methods for elucidation and observation of interfacial interactions is critical for robust investigations. In its current form, this approach provides a qualitative assessment of interfacial epitope interactions, and without peptide synthesis is not able to derive quantitative interaction data. Furthermore, variability in proteolysis kinetics of different proteins can impact sequence coverage. However, we anticipate that this approach could be applied as an efficient triaging tool to inform targeted peptide synthesis, phage library construction and scanning mutagenesis experiments, for full characterisation of transient PPI interfaces. Similarly, this approach can act as a powerful orthogonal method to improve the efficiency of other common structural methodologies to provide structural insight into the plethora of biologically relevant transient PPIs and support structure-based drug design of PPI modulators.

**Acknowledgments**

Authors acknowledge support from the BBSRC (Grant No. BB/R013993/1), The University of Cape Town, Rhodes University, the South African Research Chairs Initiative of the Department of Science and Innovation (DSI) and NRF (Grant No. 98566), the NRF CPRR (Grant No 129262), and Future Leaders – African Independent Research (FLAIR), a partnership between the AAS and the Royal Society that is funded by the UK Government as part of the Global Challenge Research Fund (GCRF).

## Figures

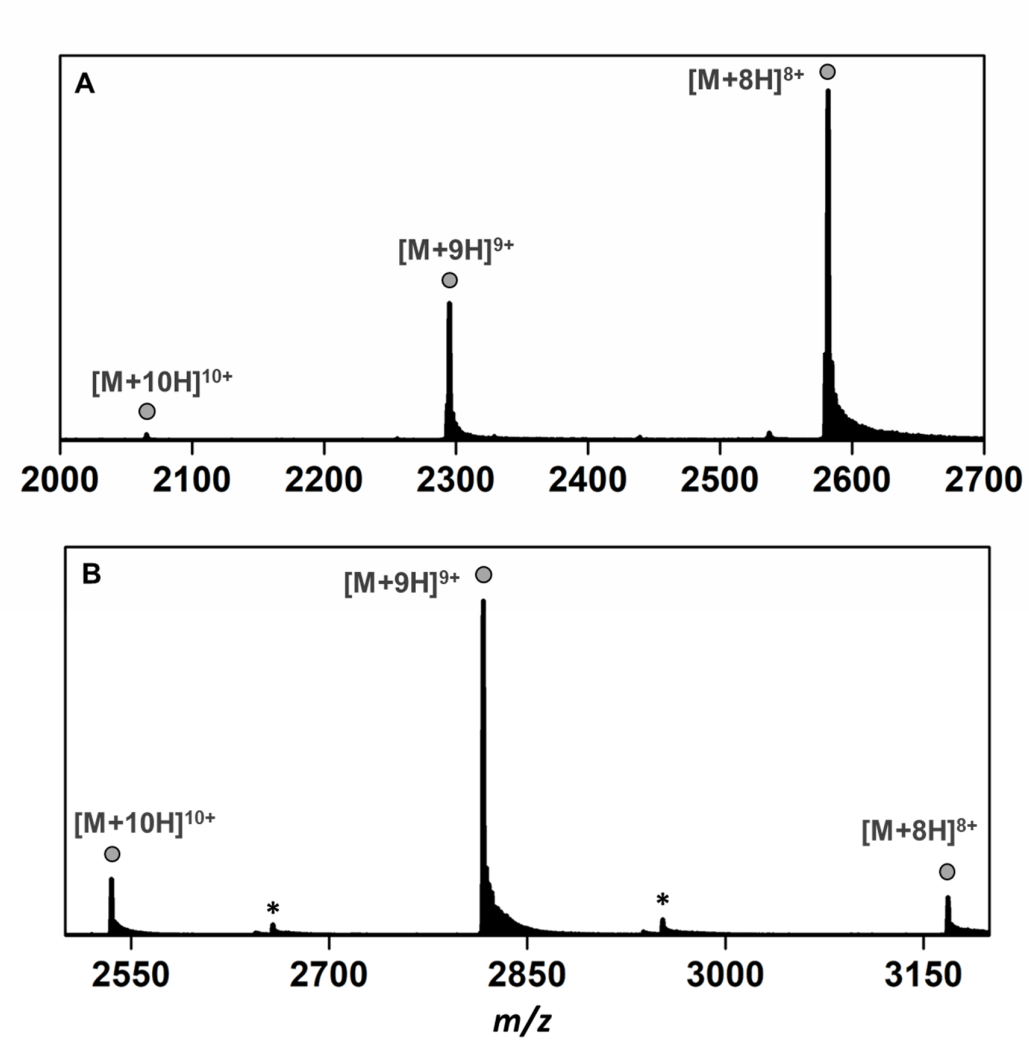


**Figure 1A:** Charge state distribution of apo TPR2A in the native state (*m/z* 2064.4, $[M+10H]^{10+}$; *m/z* 2293.6, $[M+9H]^{9+}$; *m/z* 2580.2, $[M+8H]^{8+}$. **B:** Charge state distribution of apo GrpE in the native state (*m/z* 2533.6, $[M+10H]^{10+}$; *m/z* 2814.9, $[M+9H]^{9+}$; *m/z* 3166.7 $[M+8H]^{8+}$. *Unidentified contaminants.

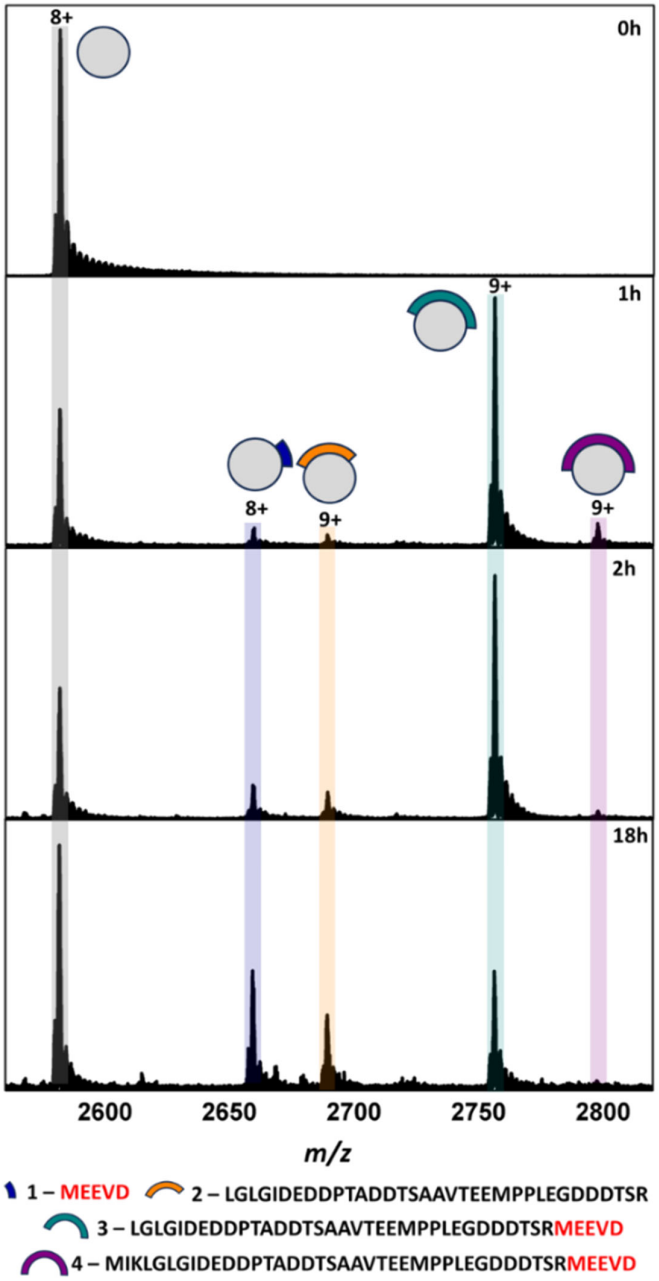


**Fig. 2. Top:** Native mass spectra of apo TPR2A (0h) and TPR2A incubated with HSP90 C-terminal peptides derived from 1h, 2h and 18h of tryptic digestion. In addition to apo TPR2A (m/z 2580.2, $[M+8H]^{8+}$), TPR2A complexes can be observed for three MEEVD con TPR2A complexes can be observed for three MEEVD-containing peptides (m/z 2657.8, $[M•\mathbf{1}+8H]^{8+}$; m/z 2754.7, $[M•\mathbf{3}+9H]^{9+}$; m/z 2796.0 $[M•\mathbf{4}+9H]^{9+}$) and one without MEEVD (m/z 2687.7 $[M•\mathbf{2}+9H]^{9+}$). **Bottom:** Peptide sequence key.

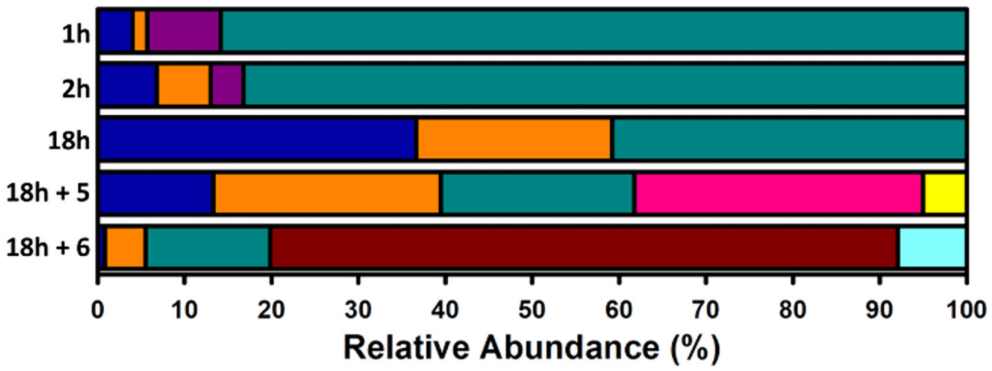


**Fig. 3.** Ratiometric analysis of the alteration of TPR2A – **1** (blue), TPR2A – **2** (orange), TPR2A – **3** (cyan) and TPR2A – **4** (purple) complexes over the experimental time course, and in the presence of peptides **5** and **6**. The addition of peptide **5**, resulted in the formation of two new complexes (TPPR2A – **5** pink and TPR2A – **5 + 2**, yellow), which had a moderate effect on the abundances of the TPR2A – **1** and TPR2A – **3** complexes, and no depletion of the TPR2A – **2** complex. The presence of peptide **6** also formed two new complexes (TPPR2A – **6**, mauve and TPR2A – **6 + 2**, light blue). However, peptide **6** significantly reduced the abundance of TPR2A complexes with peptides **1**, **2** and **3**.

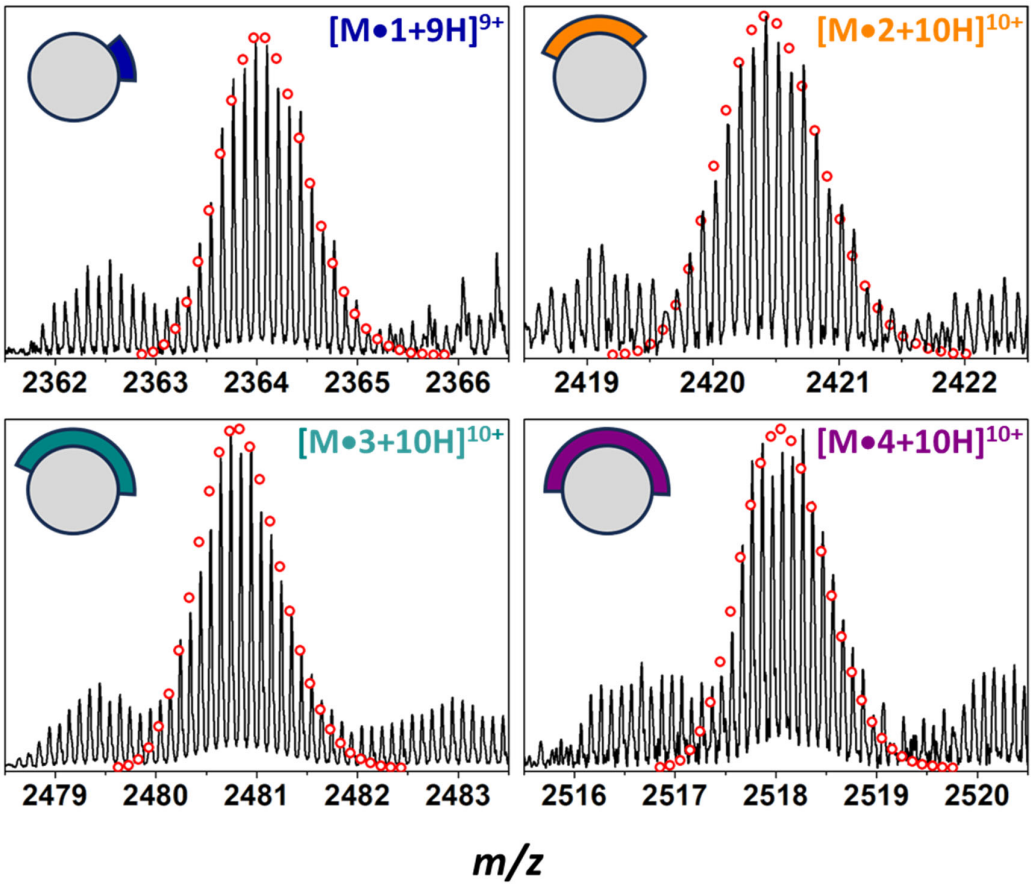


**Fig. 4.** High-resolution ESI FT-ICR MS analysis of the isotope distributions of TPR2A in complex with peptides **1 – 4**. For each species, the calculated theoretical isotope distribution for the TPR2A-peptide complex is overlaid as a scatterplot and are representative of the following molecular formulae: 1. $[C_{937}H_{1474}N_{264}O_{288}S_7 + 9H]^{9+}$; 2. $[C_{1057}H_{1662}N_{296}O_{341}S_7 + 10H]^{10+}$; 3. $[C_{1081}H_{1699}N_{301}O_{352}S_8 + 10H]1^{10+}$; 4. $[C_{1098}H_{1731}N_{305}O_{355}S_9 + 10H]^{10+}$.These data facilitated unambiguous Δ *m/z* assignment and binding peptide identification.

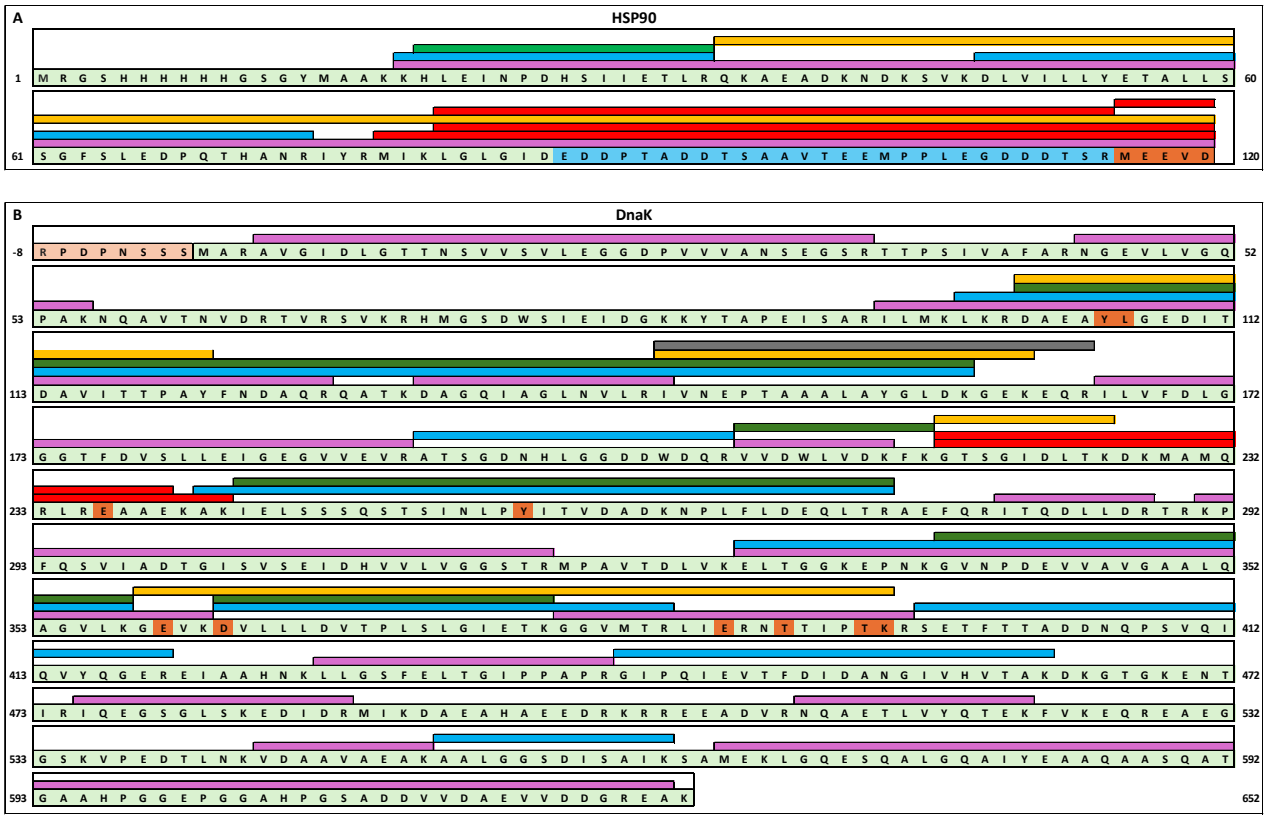


**Fig. 5.** Depiction of the sequence overage of peptides derived from tryptic digestion of HSP90-C (**A**) and DnaK (**B**) respectively. Peptides coloured red indicate binding to either TPR2A (**A**) or GrpE (**B.**). Colours used for non-binding peptides are varied, only for the purposes of figure clarity. **A**) Residues highlighted in orange, indicate known interfacial associating epitope (MEEVD). Residues highlighted in blue, correlate with previously unreported TPR2A interacting region. **B**). Residues highlighted in orange, correlate to those mutated by Li and co-workers to assess influence of various contact areas of the DnaK-GrpE PPI.[22]

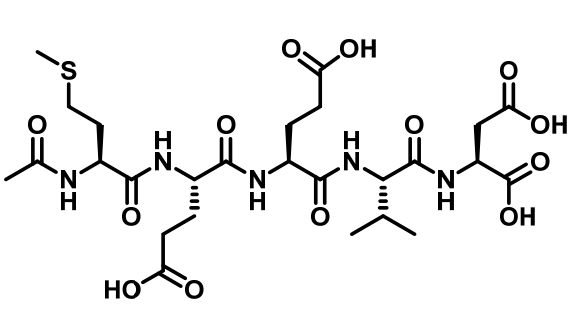

**5. Ac-MEEVD-OH**

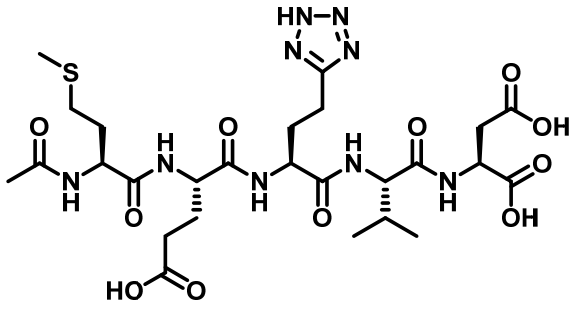

**6. Ac-METrVD-OH**

**Figure 6.** Competitively binding peptides **5** and **6**

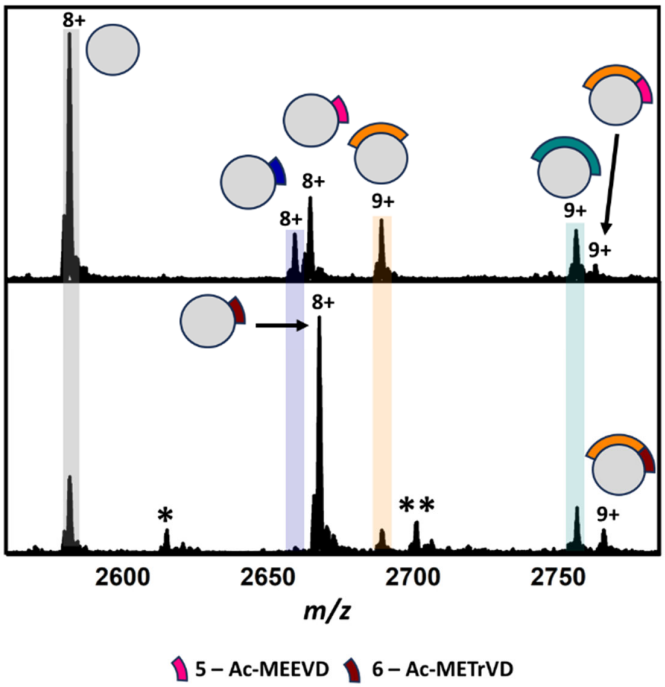


**Fig. 7. Top:** Native mass spectra of TPR2A co-incubated with HSP90 C-terminal peptides derived from an 18h tryptic digestion and peptide **5** (top) or **6** (bottom). New peaks corresponding to complexes between TPR2A and peptides **5** (m/z 2663.1, [M•**5**+8H]$^{8}$+ and **6** (m/z 2666.1, [M•**6**+8H]$^{8+}$) can be observed alongside ternary complexes between TPR2A with both peptide **2** and **6** (m/z 2761.2, [M•**2**•5+9H]$^{9+}$) or **2** and **6** (m/z 2763.9, [M•**2**•**6**+9H]$^{9+}$). **Bottom:** Peptide sequence key. * Unidentified contaminants.

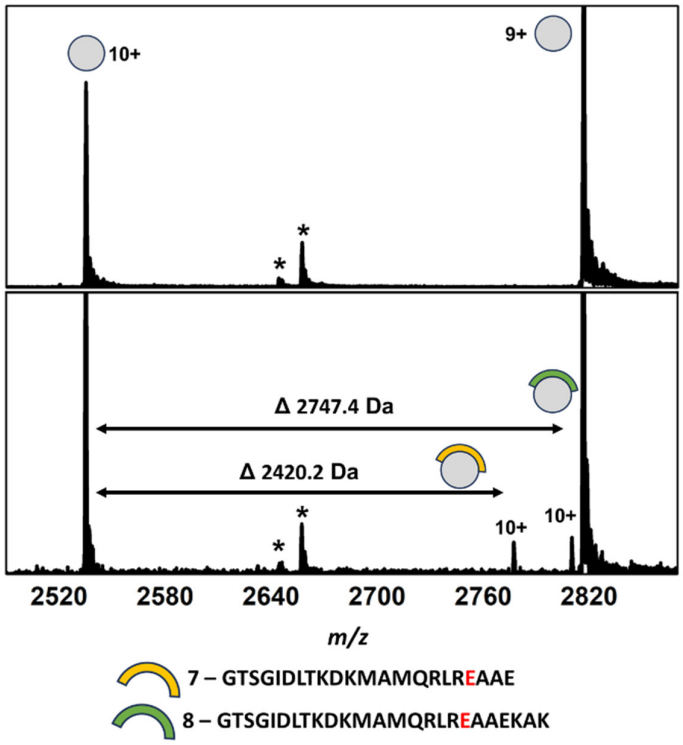


**Fig. 8.** Native mass spectra of apo GrpE (top) and co-incubated with a crude mixture of DnaK peptides derived from an 18h tryptic digestion (bottom). New peaks corresponding to complexes between GrpE and peptides **7** (m/z 2775.6, [M•**7**+10H]$^{10}$+ and **8** (m/z 2808.3, [M•8+10H]$^{10+}$) can be observed alongside apo GrpE (m/z 2533.6, [M+10H]$^{10+}$; 2814.9, [M+9H]$^{9+}$. * Unidentified contaminants.

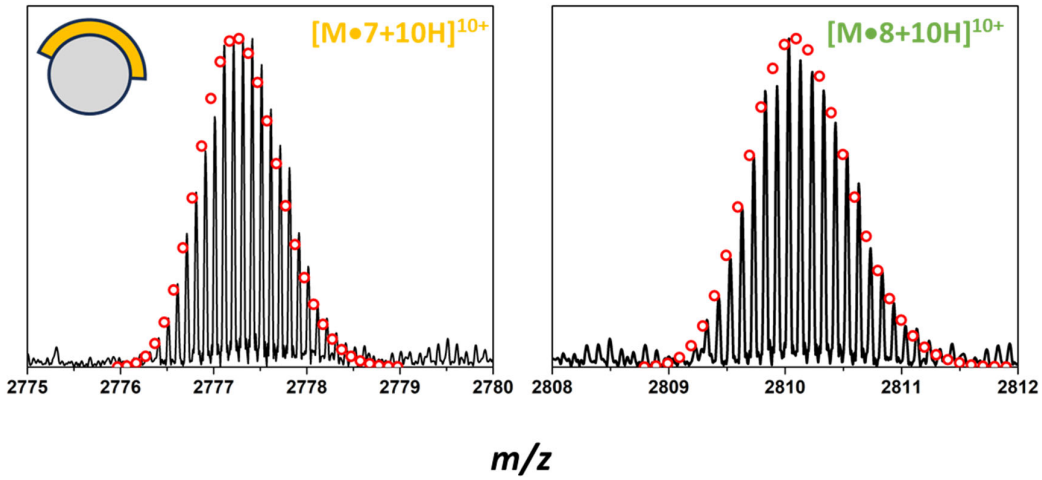


**Fig. 9.** High-resolution ESI FT-ICR MS analysis of the isotope distributions of GrpE in complex with peptides **7** and **8**. For each species, the calculated theoretical isotope distribution for the GrpE-peptide complex is overlaid as a scatterplot and are representative of the following molecular formulae: 1. $[C_{1165}H_{18174}N_{355}O_{423}S_4 + 10H]^{10+}$; 2. $[C_{1210}H_{1916}N_{2360}O_{426}S_4 + 10H]^{10+}$. These data facilitated unambiguous Δ *m/z* assignment and binding peptide identification.

## Experimental Procedures

### 1. Protein expression and purification

His-tagged TPR2A domain of human HOP and the His-tagged human HSP90αC domain were produced in the *E. coli* BL21(DE3) Codon+ strain from the pQE80L plasmid with an N-terminal hexahistidine tag. For both proteins, the transformed bacterial culture was grown in 2xYT medium [1.6 % (w/v) tryptone, 1 % (w/v) yeast extract and 0.5 % [w/v] NaCl)) to an $OD_{600}$ of 0.6, and protein production was induced with 0.5 mM isopropyl β- d-1-thiogalactopyranoside (IPTG) for 18 hours at 25°C. Cells were harvested at 6000x*g* for 15 minutes at 4°C, and the cell pellets were resuspended in His lysis buffer [50 mM $NaH_2PO_4$ pH 7.5, 300 mM NaCl, with 1 mg/ml lysozyme, 0.1 % (w/v) Triton-X and 1 mM phenylmethylsulphonyl fluoride (PMSF)]. The cell lysates were centrifuged at 16000x*g* for 30 mins at 4°C, and the supernatants were loaded onto $Ni^{+2}$-charged HisPur™ Ni-NTA Resin (Thermo Fisher Scientific, Cat # 88222), followed by overnight incubation at 4°C on a rocker. Washing was performed with cold wash buffer (50 mM $NaH_2PO_4$ pH 7.5 300 mM NaCl) containing 2-5 mM imidazole, and proteins were eluted with cold elution buffer (50 mM $NaH_2PO_4$ pH7.5, 300 mM NaCl, 200 mM imidazole). Eluted proteins were buffer exchanged into storage buffer (25 mM $NaH_2PO_4$ pH 7.5, 150 mM NaCl, 150 mM KCl) using a 3 kDa MWCO filter prior to downstream analysis. *Mycobacterium tuberculosis* (Mtb) DnaK and GrpE proteins were produced in *E. coli* BL21 (DE3) Codon+ strain as fusion proteins with an N-terminal His-SUMO tag from the pCA258 backbone (a kind gift of Matthias Mayer, ZMBH, Heidelberg). His-SUMO-DnaK and His-SUMO-GrpE proteins were purified by Ni-NTA chromatography as described above and buffer exchanged into storage buffer (25 mM $NaH_2PO_4$ pH 7.5, 150 mM NaCl, 150 mM KCl). The His-SUMO tag was removed by addition of His-tagged SUMO protease (purified in house) for 4 hours at 4 ºC with gentle rotation. Protein mixtures were subjected to a second round of Ni-NTA chromatography to remove the SUMO protease and His-SUMO tag, and then passed through a 10 kDa MWCO filter to obtain untagged DnaK and GrpE proteins.

### 2. Sample Preparation

#### a. Protein desalting

TPR2A, HSP90-C, DnaK and GrpE samples were subjected to two rounds of buffer exchange into 100 mM $NH_4OAc$ using Zeba Spin Desalting Column (Thermo Fisher Scientific). Concentration of all proteins ere adjusted to stock solutions of 250 µM.

#### b. HSP90-C digestion

100 µL of agarose supported trypsin (Thermo Fischer) was washed three times with 500 µL $NH_4OAc$ buffer (100 mM), and finally resuspended in 200 µL of the same $NH_4OAc$ buffer. 50 µL of the desalted HSP90-C or DnaK stock

solutions (250 μM) were added to this trypsin suspension. The mixture was incubated at 37 °C on a shaking heat block. Digest aliquots were removed at indicated intervals and used directly for native MS analysis.

**c. Preparation of Peptide 10 and 11 stocks**

Stock solutions (250 μM) of peptides **5** and **6** were prepared in 100 mM $NH_4OAc$.

**d. Sample preparation for Native MS**

**TPR2A-HSP90C:** In all instances 1 μL of the TPR2A stock (250 μM) was utilised for analysis and made up to a final volume of 20 μL (final protein concentration 12.5 μM). HSP90-C peptide binding experiments were prepared by mixing 2 μL aliquots of the digest mixtures with 1 μL of the TPR2A stock, and 17 μL of 100 mM $NH_4OAc$. Similarly, binding competition samples were prepared HSP90-C peptide binding experiments were prepared by mixing 2 μL aliquots of the digest mixtures with 1 μL of the peptide stock solution (final conc. 12.5 μM) 1 μL of the TPR2A stock, and 16 μL of 100 mM $NH_4OAc$.

**GrpE-DnaK:** 2 μL of the GrpE stock (250 μM) was utilised for analysis and made up to a final volume of 20 μL (final protein concentration 25 μM). DnaK peptide binding experiments were prepared by mixing 4 μL aliquots of the digest mixtures with 2 μL of the GrpE stock, and 14 μL of 100 mM $NH_4OAc$.

All samples were made up in 96-well plates and held at 4 °C prior to MS analysis.

## 3. Mass Spectrometry

Native MS were obtained on a 12T SolariX 2XR FT-ICR (Bruker Daltonics). Ionisation was achieved using a NanoMate nESI infusion robot (TriVersa Biosciences), sampling from a 96-well plate. Typically, a nanoelectrospay voltage of 1.55 kV was used and backing pressure was adjusted to maintain stable electrospray. Typically, spectra were acquired as the sum of 200 1 MegaWord FID transients. DataAnalysis software (Bruker Daltonics) was used for native MS analysis. LC-MS data was acquired on a Synpat q-TOF, coupled to an Acquity UPLC (Waters). Solvent A (0.1% TFA in $H_2O$) and solvent B (0.1% TFA in $CH_3CN$) were set at 95% (A) and 5% (B) with a gradient running to 5% (A) and 95% (B) over 20 minutes. LC-MS data were processed using MassLynx v4.0 (Waters)

## 4. Data Analysis

For each spectrum a mass list and accompanying peak areas was generated using the FTMS algorithm (S/N threshold of 5). Protein – Peptide complexes were identified via $\Delta m/z$ as compared to apo protein at each charge state (**Table S1**). The area of each peak corresponding to of an TPR2A-peptide complex from each of the three native charge states (10+, 9+ and 8+) was combined. TPR2A-peptide association was calculated from the summed peak area of for each species as a percentage of the total peak area for each species and charge state (**Table S2**) Figures are the average of two replicates.

A list of possible tryptic cleavage products was generated using Expasy PeptideMass[24] with missed cleavages set to 5. The crude mixture following 18 hours of tryptic digestion was subjected to UPLC-MS, where tryptic cleavage product were identified by their mass signature (**Figure S3**).

## 5. Supplementary Tables and Figures

**Table S1.** Δ*m/z* of TPR2A and GrpE binding peptides

| | | | Monoisotopic mass | Δ*m/z* 10+ | 9+ | 8+ |
|---|---|---|---|---|---|---|
| HSP90 | Peptide 1 | MEEVD | 621.23 | 62.123 | 69.03 | 77.65 |
| | Peptide 2 | LGLGIDEDDPTADDTSAAVTEEMPPLEGDDDTSR | 3546.53 | 354.653 | 394.06 | 443.32 |
| | Peptide 3 | LGLGIDEDDPTADDTSAAVTEEMPPLEGDDDTSRMEEVD | 4149.75 | 414.98 | 461.08 | 518.72 |
| | Peptide 4 | MIKLGLGIDEDDPTADDTSAAVTEEMPPLEGDDDTSRMEEVD | 4521.97 | 452.20 | 502.44 | 565.25 |
| | Peptide 5 | Ac-MEEVD-OH | 663.24 | 66.32 | 73.69 | 82.91 |
| | Peptide 6 | Ac-METrVD-OH | 687.26 | 68.73 | 76.36 | 85.91 |
| DnaK | Peptide 7 | GTSGIDLTKDKMAMQRLREAAE | 2420.2 | 242.0 | 268.9 | |
| | Peptide 8 | GTSGIDLTKDKMAMQRLREAAEKAK | 2747.4 | 274.7 | 305.3 | |

**Table S2 -** Peak areas of each TPR2A - peptide complex at 10+ 9+ and 8+ charge states

**TPR2A and 1-hour trypsin digest**

| Associating Peptide | Peak Area 10+ | 9+ | 8+ | Sum for each complex | Complexation ratio (%) |
|---|---|---|---|---|---|
| Peptide 1 | 0 | 1053439 | 910818 | **1964257** | **4.04** |
| Peptide 2 | 188027 | 628819 | 0 | **816846** | **1.68** |
| Peptide 3 | 8164246 | 20644026 | 12853107 | **41661379** | **85.8** |
| Peptide 4 | 1476830 | 1406567 | 1219093 | **4102490** | **8.45** |
| **Sum for each charge state** | **9829103** | **23732851** | **14983018** | | |
| | | **Total** | **48544972** | | |

**TPR2A and 2-hour trypsin digest**

| Associating Peptide | Peak Area 10+ | 9+ | 8+ | Sum for each complex | Complexation ratio (%) |
|---|---|---|---|---|---|
| Peptide 1 | 215006 | 2599536 | 4124846 | **6939388** | **6.81** |
| Peptide 2 | 849615 | 3284724 | 2160752 | **6295091** | **6.17** |
| Peptide 3 | 18174782 | 39100112 | 27607906 | **84882800** | **83.2** |
| Peptide 4 | 1024690 | 1442473 | 1376475 | **3843638** | **3.77** |
| **Sum for each charge state** | **20264093** | **46426845** | **35269979** | | |
| | | **Total** | **101960917** | | |

**TPR2A and 18-hour trypsin digest**

| Associating Peptide | Peak Area 10+ | 9+ | 8+ | Sum for each complex | Complexation ratio (%) |
|---|---|---|---|---|---|
| Peptide 1 | 284422 | 3199550 | 2600608 | **6084580** | **36.6** |
| Peptide 2 | 640074 | 1980404 | 1131010 | **3751488** | **22.6** |
| Peptide 3 | 1163291 | 4407053 | 1198269 | **6768613** | **40.8** |
| Peptide 4 | 0 | 0 | 0 | **0** | **0** |
| **Sum for each charge state** | **2087787** | **9587007** | **4929887** | | |
| | | **Total** | **16604681** | | |

**TPR2A and 18-hour trypsin digest + Ac-MEEVD-OH**

| Associating Peptide | Peak Area 10+ | 9+ | 8+ | Sum for each complex | Complexation ratio (%) |
|---|---|---|---|---|---|
| Peptide 1 | 290112 | 903797 | 2360950 | **3554859** | **13.3** |
| Peptide 2 | 1505832 | 3548110 | 1939216 | **6993158** | **26.1** |
| Peptide 3 | 1634420 | 2858139 | 1455786 | **5948345** | **22.3** |
| Ac-MEEVD-OH | 275890 | 797004 | 275890 | **1348784** | **33.2** |
| Ac-MEEVD-OH + Peptide 2 | 445425 | 4853345 | 3570962 | **8869732** | **5.05** |
| **Sum for each charge state** | **4151679** | **12960395** | **9602804** | | |
| | | **Total** | **26714878** | | |

**TPR2A and 18-hour trypsin digest + Ac-METrVD-OH**

| Associating Peptide | Peak Area 10+ | 9+ | 8+ | Sum for each complex | Complexation ratio (%) |
|---|---|---|---|---|---|
| Peptide 1 | 0 | 219919 | 0 | **219919** | **0.847** |
| Peptide 2 | 0 | 736447 | 481048 | **1217495** | **4.69** |
| **Peptide 3** | 705668 | 2207969 | 804376 | **3718013** | **14.3** |
| Ac-METrVD-OH | 573528 | 10035904 | 8152358 | **18761790** | **72.2** |
| Ac-MEEVD-OH + Peptide 2 | 357600 | 1138675 | 558534 | **2054809** | **7.91** |
| **Sum for each charge state** | **1636796** | **14338914** | **9996316** | | |
| | | **Total** | **25972026** | | |

## References


1. De Keersmaecker, H. *et al.* Mapping Transient Protein Interactions at the Nanoscale in Living Mammalian Cells. *ACS Nano* **12**, 9842–9854 (2018).
2. Perkins, J. R., Diboun, I., Dessailly, B. H., Lees, J. G. & Orengo, C. Transient Protein-Protein Interactions: Structural, Functional, and Network Properties. *Structure* **18**, 1233–1243 (2010).
3. Jubb, H., Higueruelo, A. P., Winter, A. & Blundell, T. L. Structural biology and drug discovery for protein-protein interactions. *Trends Pharmacol. Sci.* **33**, 241–248 (2012).
4. Nevola, L. & Giralt, E. Modulating protein-protein interactions: The potential of peptides. *Chem. Commun.* **51**, 3302–3315 (2015).
5. Cunningham, J. M., Koytiger, G., Sorger, P. K. & AlQuraishi, M. Biophysical prediction of protein–peptide interactions and signaling networks using machine learning. *Nat. Methods* **17**, 175–183 (2020).
6. Acuner Ozbabacan, S. E., Engin, H. B., Gursoy, A. & Keskin, O. Transient protein-protein interactions. *Protein Eng. Des. Sel.* **24**, 635–648 (2011).
7. Plata, M., Sharma, M., Utz, M. & Werner, J. M. Fully Automated Characterization of Protein-Peptide Binding by Microfluidic 2D NMR. *J. Am. Chem. Soc.* **145**, 3204–3210 (2023).
8. Leney, A. C. & Heck, A. J. R. Native Mass Spectrometry: What is in the Name? *J. Am. Soc. Mass Spectrom.* **28**, 5–13 (2017).
9. Bennett, J. L., Nguyen, G. T. H. & Donald, W. A. Protein-Small Molecule Interactions in Native Mass Spectrometry. *Chemical Reviews* vol. 122 7327–7385 (2022).
10. Tamara, S., Den Boer, M. A. & Heck, A. J. R. High-Resolution Native Mass Spectrometry. *Chem. Rev.* **122**, 7269–7326 (2022).
11. Veale, C. G. L. *et al.* A native mass spectrometry platform identifies HOP inhibitors that modulate the HSP90–HOP protein–protein interaction. *Chem. Commun.* **57**, 10919–10922 (2021).
12. Bellamy-Carter, J. *et al.* Discovering protein-protein interaction stabilisers by native mass spectrometry. *Chem. Sci.* **12**, 10724–10731 (2021).
13. Fiorentino, F., Rotili, D., Mai, A., Bolla, J. R. & Robinson, C. V. Mass spectrometry enables the discovery of inhibitors of an LPS transport assemblyviadisruption of protein-protein interactions. *Chem. Commun.* **57**, 10747–10750 (2021).
14. Vaaltyn, M. C. *et al.* Native mass spectrometry guided screening identifies hit fragments for HOP-HSP90 PPI inhibition. *ChemBioChem* **21**, e202200322 (2022).
15. Katz, C. *et al.* Studying protein–protein interactions using peptide arrays. *Chem. Soc. Rev.* **40**, 2131–2145 (2011).
16. Clarke, D. J., Murray, E., Hupp, T., MacKay, C. L. & Langridge-Smith, P. R. R. Mapping a Noncovalent Protein – Peptide Interface Using Electron Capture Dissociation. *J. Am. Soc. Mass Spectrom.* **22**, 1432–1440 (2011).
17. Seo, M. H., Nim, S., Jeon, J. & Kim, P. M. Large-scale interaction profiling of protein domains through proteomic peptide-phage display using custom peptidomes. in *Methods in Molecular Biology* vol. 1518 213–226 (2017).
18. Lu, X., DeFelippis, M. R. & Huang, L. Linear Epitope Mapping by Native Mass Spectrometry. *Anal. Biochem.* **395**, 100–107 (2009).
19. Wang, R. Y. R. *et al.* Structure of Hsp90–Hsp70–Hop–GR reveals the Hsp90 client-loading mechanism.

*Nature* **601**, 460–464 (2022).

20. Veale, C. G. L. *et al.* Modulators of the Hop-HSP90 Protein-Protein Interaction Disrupt Early-Stage of KSHV Lytic Replication. *ChemRxIV* 10.26434/chemrxiv-2024-2q612 (2024).
21. Lupoli, T. J., Vaubourgeix, J., Burns-Huang, K. & Gold, B. Targeting the Proteostasis Network for Mycobacterial Drug Discovery. *ACS Infect. Dis.* **4**, 478–498 (2018).
22. Xiao, X. *et al.* Structure of the M. tuberculosis DnaK−GrpE complex reveals how key DnaK roles are controlled. *Nat. Commun.* **15**, 660 (2024).
23. Chang, L. & Perez, A. Ranking Peptide Binders by Affinity with AlphaFold**. *Angew. Chemie - Int. Ed.* **62**, e202213362 (2023).
24. Wilkins, M. R. *et al.* Detailed peptide characterization using PEPTIDEMASS – a World-Wide-Web-accessible tool. *Electrophoresis* **18**, 403–408 (1997).